Solvation of the methoxy radical in small clusters

J. A. Fernandez, J. Yao, and E. R. Bernstein

Solvation of the methoxy radical in small clusters

J. A. Fernandez, J. Yao, and E. R. Bernstein
Department of Chemistry, Colorado State University, Fort Collins, Colorado 80523-1872

In this work we analyze clusters between the methoxy radical (CH_3O, an open-shell molecule) and the nonpolar solvents Ar, N_2, CH_4, and CF_4. CH_3O is formed through the photolysis of CH_3OH vapor in a supersonic expansion of CH_3OH and a solvent gas (Ar, N_2, CH_4, CF_4) seeded in a carrier gas of He. The radical and solvent molecules are cooled to $\sim 15-20$ K and form clusters. These clusters are probed using laser induced fluorescence (LIF) of the CH_3O radical. An extensive set of calculations, including *ab initio* and atom–atom potential calculations and rotational contour simulations are performed for each cluster in order to elucidate the cluster structure and the nature and relative importance of the limiting types of interactions that are responsible for cluster binding. A final minimum energy structure is presented for each cluster, together with the analysis of the limiting type of interactions that generate the van der Waals binding of the cluster. © 1997 American Institute of Physics. [S0021-9606(97)01033-7]

I. INTRODUCTION

The study of van der Waals clusters serves many purposes; intra- and intermolecular dynamics,[1] energy transfer,[2] unimolecular dissociation,[3] solvation,[4] chemical reactions,[5] potential energy surfaces,[6] collisional processes,[7] and molecular orientation during collisions[8] can all be studied through the spectroscopy of van der Waals clusters.

Experimental determination of cluster structure is by no means a simple task. Clusters are more often than not highly nonrigid,[9] and this characteristic is often quite difficult to ascertain in the observed spectrum.[10] Calculations of cluster structure also present a number of difficulties at the level of either semiempirical or *ab initio* theory. At the semiempirical, potential energy surface level, one must determine the nature and form of the potential or force term that must be considered for the pairwise interactions. These can include a number of different terms depending on the nature of the molecules comprising the cluster or system (e.g., multipolar, dispersion, hydrogen bonding, charges, charge-transfer). Potential terms are often of an atom–atom type with forms such as Lennard-Jones,[11] Morse,[12] exponential-six,[13] or more specialized versions for particular systems.[14,15]

Open shell molecules or radicals can present especially difficult problems for such cluster-interaction studies; nonetheless, such systems are of particular importance because they are central to much of the chemistry active in all three phases of matter. Because of the open shell structure of radicals, their interaction with other molecules can be quite strong; some systems display interactions whose strengths can fall between those of electrostatic interactions and chemical bonds.[16] Success in modeling these strong interactions of open shell species with simple molecules will shed light on the nature of their reactions and energy transfer processes.

In this report, we present data for the important and well studied[17] combustion species, the methoxy radical CH_3O, solvated by Ar, N_2, CH_4, and CF_4 in van der Waals clusters. The apparent simplicity of these cluster systems notwith-

standing, they present a rich variety of structures, interactions, and dynamics. In these van der Waals clusters, the solute CH_3O is an open shell system with an unpaired electron in an almost pure oxygen $2p$ orbital. Several theoretical[18] and experimental[19] studies have addressed the Jahn–Teller distortion and dissociative properties of the methoxy radical.

van der Waals complexes containing even simple radicals are often difficult to model because the nature of the interactions between the radical and the solvent molecules can be very specific and solvent molecule dependent; for example, the CH_3O/Ar cluster interactions should have major contributions from dispersion and charge transfer terms,[20] the CH_3O/N_2 cluster interactions should have major contributions from quadrupole terms;[21] the CH_3O/CF_4 cluster interactions should have major contributions from Coulombic terms, and the CH_3O/CH_4 clusters interactions can have contributions from reaction processes. A unique form, into which these various detailed interactions can be cast, is often difficult to find. Data obtained from electronic spectroscopy of such clusters can be employed to evaluate the interactions, structure, and energy levels of solvated radicals. In these studies we employ a Lennard-Jones–Coulomb atom–atom potential form to model the geometries, energetics, and normal modes of CH_3O/Ar, N_2, CF_4, CH_4 clusters. This type of empirical potential energy surface calculation gives qualitative (and in some instances quantitative) descriptions of cluster structures, binding energies, and van der Waals mode frequencies.

An alternative approach would be to use *ab initio* quantum theory to model cluster properties and potential energy surfaces; physical chemists are presently learning how to accomplish this through large correlation corrected basis sets and extensive configuration interaction techniques. This fundamental and essential approach does, however, tend to limit our ability to generalize the overall complex cluster interaction surface into particular limiting, useful, and informative functional forms.

The elucidation of cluster structure and energetics pro-

ceeds from the laser induced fluorescence spectroscopy of methoxy radical clusters. These data yield rotational envelopes, vibrational energy (van der Waals and molecular), and free molecule-to-cluster energy shifts for 1:1 and 1:2 CH_3O/solvent clusters. These spectroscopic results are then modeled through a combination of *ab initio*, potential energy surface, normal mode, and rotational envelope calculations. Through comparisons of experimental results with the models, cluster binding energies, structures, and van der Waals modes are determined.

For the clusters discussed in this paper, the presented calculations find that two cluster minimum energy conformations, with similar binding energies, are available to each CH_3O(solvent)$_1$ species. The identification of one of these structures with the experimental results is made through a comparison between predicted and observed spectroscopic shifts, vibrational frequencies, and rotational contours of the cluster vibronic transitions. Based on these determinations, the relative contributions of different interactions to the cluster potential surface are briefly discussed.

II. PROCEDURES

A. Experiment

The experimental setup has been described elsewhere.[21,22] Briefly, the experiments have been carried out in a stainless steel vacuum chamber at a pressure of $\sim 10^{-4}$ Torr. To produce the clusters, CH_3OH vapor is mixed with He carrier gas and the clustering agent. The mixture passes through a pulsed valve (General Valve 0.7 mm nozzle diameter) and expands in the chamber, producing both cooling and cluster formation. Typical pressures and concentrations vary from one solvent to another, but are in the range of 150–500 psi for the expansion gas with a stagnation pressure concentration of 10%–20% for the solvent gas. Cooling is one of the most critical parameters in this study. CH_3OH photolysis produces extremely hot radicals. The vibrational-translational energy transfer process that cools the CH_3O radical is not very efficient, due to the radical's high vibrational frequencies;[23] many collisions are required to reach the low temperature necessary for the cluster formation process to take place. Higher stagnation pressures are then required if compared to those needed for the cooling and clustering of stable molecules.[4]

An ArF excimer laser (193 nm), with output power of ~ 80 mJ/pulse, aligned collinearly with the supersonic expansion axis and focused with a 15 cm lens is used to photolyze the methanol precursor and produce the radicals. The nozzle has a 1 cm×1 mm quartz tube at its exit which confines both the laser and molecular beams as the nozzle opens. The excimer light is aligned so as not to ablate the polymer poppet that opens and closes the pulsed nozzle. The photolysis of CH_3OH occurs within this quartz tube. Cooling of CH_3O below 300 K and cluster formation occur as the gas (He, CH_3O, solvent) expands from the quartz tube into the vacuum chamber. A second laser (a Nd/YAG-dye couple system) is used to probe the radicals about 2 cm downstream from the tube. The fluorescence emission is collected perpen-

dicularly to the laser/molecular jet plane and detected by a C31034A RCA photomultiplier tube. A U330 filter is employed to attenuate scattered light from the excimer laser.

B. Theory

In order to understand and analyze the experimental results, an extensive series of calculations is performed on each solute/solvent system.

Cluster structure is determined by employing a potential energy calculation based on an atom–atom Lennard-Jones Coulomb potential energy function.[9,24] The program considers the molecules as rigid entities during cluster formation, and determines the interaction energy as a sum of different terms: short range repulsion, induction/dispersion, electrostatic, hydrogen bonding, etc. The potential energy surface for the interaction between the atoms is given by[25–28]

$$E = \sum_{i=1}^{n} \sum_{j=1}^{m} \left[\left(\frac{A_{ij}}{r_{ij}^{12}} - \frac{C_{ij}}{r_{ij}^{6}} \right)(1 - \delta_{ij}^{hb}) + \frac{q_i q_j}{D r_{ij}} \right.$$
$$\left. + \left(\frac{A_{ij}^{hb}}{r_{ij}^{12}} - \frac{C_{ij}^{hb}}{r_{ij}^{10}} \right) \delta_{ij}^{hb} \right] \tag{1}$$

in which

$$A_{ij} = C_{ij} r_{\min}^{6}/2 \quad \text{and} \quad C_{ij} = \frac{(3/2)e(\hbar/m^{1/2})\alpha_i a_j}{(\alpha_i/N_i)^{1/2} + (\alpha_j/N_j)^{1/2}}, \tag{2}$$

m is the electronic mass, δ_{ij} is 1 when the atoms can form hydrogen bonds and 0 in the rest of the cases, q_i, q_j are the atomic charges, D is the dielectric constant, $r_{\min}$ is the sum of van der Waals radii and is different for each pair of atoms, α_i are the atomic polarizabilities and are evaluated from experimental data, N_i is the effective number of electrons for each atom type, and r_{ij} is the distance between atoms i and j of different molecules.

All the parameters in Eqs. (1) and (2) are available for the ground state systems, except the atomic charges. Atomic charges are calculated using an *ab initio* package (GAUSSIAN 94) (Ref. 29) and experimental geometries. A Mulliken population analysis is employed to determine the charge density on each atom. The charge density found for each atom is shown in Table I, together with the theory level used for its determination.

The parameters needed to formulate and solve the system of equations represented by Eqs. (1) and (2) above are not available for the excited states of molecules and radicals. Calculations provide the partial atomic charges but not the excited state atomic van der Waals radii and atomic polarizabilities. To solve this problem and obtain excited state cluster binding energies (in order to calculate cluster spectroscopic shifts) we calculate the atomic partial charges for the excited state of CH_3O and use them in the calculation of the excited state binding energy and geometry of the CH_3O(Ar)$_1$ cluster. The carbon and oxygen potential terms A_{ij} and C_{ij} are then adjusted through α_i and r_i (van der

TABLE I. Atomic partial charges, polarizabilities, and van der Waals radii for the cluster potential energy surfaces used in the atom–atom potential calculation [Eqs. (1) and (2)]. The charges and other potential parameters change on the methoxy radical with electronic excitation $A \leftarrow X$ but not on the solvent species. Atomic charges are calculated employing a Mulliken population analysis. See text for more details.

Molecule	Atom	Charge		Calculation level	α_i		r_i	
		$X\,^2E$	$A\,^2A_1$		$X\,^2E$	$A\,^2A_1$	$X\,^2E$	$A\,^2A_1$
CH_3O^a	O	-0.2245	-0.5028		0.59	0.800^e	3.24	3.10^e
	C	-0.3198	-0.1843	CASSCF(7,9)/D95	1.51	1.60^e	3.74	3.70^e
	H	0.1814	0.229		0.42	0.42^e	2.92	2.92^e
CF_4^b	C	0.9837		MP4/6-311G**	0.93		4.12	
	F	-0.2460			0.557		2.70	
CH_4^c	C	-0.08			0.93		4.12	
	H	0.02			0.42		2.92	
N_2^c	N	0.377			0.00		1.00	
	q^d	-0.377			0.00		1.00	

[a]Geometry from Ref. 30.
[b]Geometry from *Handbook of Chemistry and Physics*, 7th ed. (Chemical Rubber, Boca Raton, 1995).
[c]Geometry and charges from Ref. 14.
[d]Charges added on the molecular axis of N_2 at 0.25 Å further from the center of mass than each N atom.
[e]Estimated, see text.

Waals radius of atom i) to obtain a best fit for the gas to cluster shift for the $CH_3O(Ar)_1$ cluster. These values for A_{ij} and C_{ij} of carbon and oxygen are then used throughout the remaining excited state cluster calculations. The above approach seems more reliable at the present time than calculating atomic charges, radii, and polarizabilities for the excited states of radicals.

Excited state parameters thus obtained for the potential energy surface yield shifts that are only in some instances quantitatively correct, but are usually always of qualitative accuracy. These results for excited state cluster geometry, however, allow good rotational constants and vibrational frequencies to be generated.

The van der Waals modes of the cluster can be found by a normal coordinate analysis of the cluster employing the FG matrix method of Wilson *et al.*[30] Assuming that intramolecular vibrations are not coupled to the low-frequency intermolecular modes, this calculation will generate all the intermolecular vibrations and their eigenvectors.[31,32] Calculation of excited state frequencies will be influenced by the inaccurate determination of the excited electronic state potential energy surface and binding energy; nonetheless, the resulting frequencies can still serve as a guide for spectral assignments if the potential energy barriers between multiple equivalent minima on the potential energy surface are large with respect to the calculated ''harmonic'' mode energy.

Sometimes atom–atom potential energy surface calculations lead to more than one minimum energy structure for a cluster. The structures can exhibit binding energies that are so similar that the calculation itself is not sufficient to assign the experimental spectrum to one of the isomers. The correct cluster structural assignment can be given by a rotational contour analysis based on the calculated geometries. A program that finds the eigenvectors and eigenvalues of an asymmetric rigid rotor rotational Hamiltonian[33] is used to simulate the rotational contour for each of the studied clusters and structures. The program uses as input the laser resolution, the rotational temperature, the type of band (Hund's cases a, b, c,

or their percentages), and the rotational constants for both ground and electronic excited states based on a particular calculated cluster structure. The comparison between the calculated rotational spectrum for each cluster and the experimental data are sufficient in most of the cases to confirm unequivocally the actual cluster geometry.

III. EXPERIMENTAL RESULTS AND STRUCTURE DETERMINATION

A. Methoxy radical

The CH_3O radical geometry undergoes a large change upon electronic excitation. The first electronic state of CH_3O is formed by the excitation of an electron from a bonding carbon–oxygen orbital to a nonbonding orbital on the oxygen atom.[34] This induces the CO bond length to increase from 1.363 Å in the ground state to 1.58 Å in the excited state.[35,36] The Franck–Condon factors will then favor vibronic transitions with significant changes in the vibrational quantum numbers for the C–O vibrational excitation. The origin for the $A \leftarrow X$ electronic transition will then be very weak. This can be observed in Fig. 1, in which the CH_3O electronic spectrum is shown for the 0_0^0, 3_0^1, and 3_0^2 and 2_0^1 transitions. The ν_3 mode corresponds to the CO stretch, and the ν_2 mode corresponds to the CH_3 umbrella motion; 3^2 and 2^1 create a Fermi resonance couple.

B. Methoxy/argon

Figure 2 depicts the $CH_3O(Ar)_n$, $n = 1, 2$, spectra in the vicinity of the 0_0^0, the 3_0^1, and the 3_0^2 and 2_0^1 CH_3O transitions. In the figures and in the rest of the text, cluster transitions are indicated by a line over the transition number (for example, $\overline{3_0^1}$ corresponds to the 3_0^1 transition of the bare molecule). The doublets red shifted 29 cm^{-1} from the bare molecule peaks are due to the $CH_3O(Ar)_1$ cluster, and the doublets red shifted 55 cm^{-1} from the CH_3O peaks are due to the $CH_3O(Ar)_2$ cluster. Due to the near coincidence between
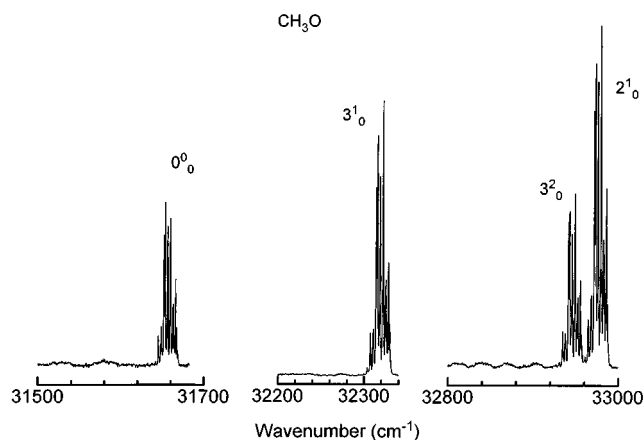
CH$_3$O

FIG. 1. LIF spectra of CH$_3$O 0_0^0, 3_0^1, 3_0^2, and 2_0^1 transitions. Despite the high backing pressure used (150 psi He) the peaks present an extensive rotational structure. Compare to Fig. 2 for which Ar is used as the expansion gas.

the 3_0^2–2_0^1 separation and the cluster shift, the strong CH$_3$O(Ar)$_1$ $\overline{2}{}_0^1$ peak lies within the CH$_3$O 3_0^2 band. This overlap can be seen by comparing the relative intensities for the 3_0^2 and 2_0^1 peaks in Figs. 1 and 2. The CH$_3$O(Ar)$_2$ $\overline{2}{}_0^1$ is again coincident with the CH$_3$O(Ar)$_1$ $\overline{3}{}_0^2$. No peak for the CH$_3$O(Ar)$_2$ $\overline{3}{}_0^2$ is detected, probably due to its low intensity. The spectra are in good agreement with those published previously.[37,38] In the earlier studies, the cluster geometry was assumed to be collinear, with the Ar atom close to the oxygen end of the CH$_3$O molecule and lying on the molecular axis. This assignment was based on the doublet nature of the unresolved rotational structure, that resembles a $P-R$ branch structure, typical of a Hund's case b molecule;[39] that is, the same type of transition as found for the bare molecule. This expectation suggests that the argon atom should be placed in the cluster such that it does not change the electronic transition dipolar moment. This condition is fulfilled
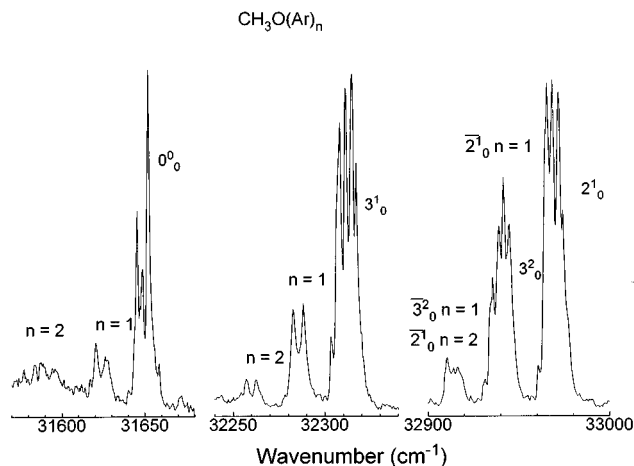
CH$_3$O(Ar)$_n$

FIG. 2. LIF spectra of CH$_3$O(Ar)$_n$, $n=1, 2$, in the vicinity of four different CH$_3$O vibronic features; 0_0^0, 3_0^1, 3_0^2, and 2_0^1. Notice that the rotational structure on the CH$_3$O vibronic transitions is much less extensive for these spectra than for those of Fig. 1. The methoxy radicals in this instance are much colder rotationally for an Ar expansion than for a He expansion.
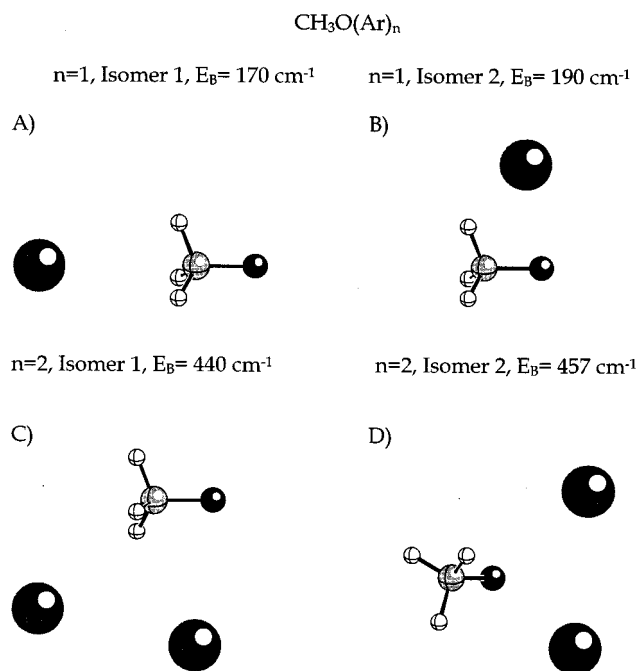
CH$_3$O(Ar)$_n$

n=1, Isomer 1, E$_B$= 170 cm^{-1} n=1, Isomer 2, E$_B$= 190 cm^{-1}

A)   B)

n=2, Isomer 1, E$_B$= 440 cm^{-1} n=2, Isomer 2, E$_B$= 457 cm^{-1}

C)   D)

FIG. 3. Calculated structures for CH$_3$O(Ar)$_1$ (a) isomer 1 and (b) isomer 2, and CH$_3$O(Ar)$_2$ (c) isomer 1 and (d) isomer 2. E_B is the cluster binding energy.

only if the Ar atom is placed on the CH$_3$O molecular axis. Powers et $al.$[37] chose the CH$_3$O oxygen end as the most probable position for the Ar atom.

As described in the previous section, an atom–atom potential calculation is carried out in this study to elucidate cluster structure. This calculation yields two different minimum energy structures, labeled as CH$_3$O(Ar)$_1$ isomers 1 and 2 in Figs. 3(a) and 3(b). For isomer 1 (calculated E_B =170 cm^{-1}, see Table II) the Ar atom is placed on the molecular axis, attracted to the H's. This is a similar structure to the one described by Powers et $al.$, but with the Ar placed in the other end of the molecule. With the level of approximation used in our work, a structure with Ar attracted to the oxygen end of CH$_3$O is not an energy minimum. For isomer 2 (calculated E_B=190 cm^{-1}) the Ar atom is placed about halfway between the carbon and oxygen atoms and above the C–O bond, probably attracted by the electron density of the σ, π C–O bond. This is the more stable isomer, but its stabilization or binding energy is very similar to that of isomer 1 (see Table II).

The excited state calculated binding energy for the CH$_3$O(Ar)$_1$ cluster is initially obtained by using the ground state values for atomic polarizabilities and van der Waals radii and the excited state partial atomic charges. This potential energy surface leads to a blue shift of 7 cm^{-1} for isomer 1 and a red shift of -1 cm^{-1} for isomer 2. Even though this calculation is successful in predicting the most stable isomer spectral shift sign, the result is quantitatively poor. As has been pointed out in the previous section, this is due to the lack of data for CH$_3$O excited state atomic polarizabilities

TABLE II. Calculated binding energies, shifts, isomerization barriers, and excited state stretching vibration frequencies for all the clusters studied. All quantities are given in cm^{-1}. The excited state parameters (polarizabilities and van der Waals radii) are adjusted for $CH_3O(Ar)_1$ isomer 2 to match the experimental results, as described in the text. The corrected parameters are then used ''as is'' for the rest of the excited state calculations (see Table I for parameters in the calculation).[a]

CH_3O	Isomer	E_B (cm^{-1})	E_B^* (cm^{-1})		Shift			σ	
			$p1$	$p2$	Expt	Calc	Barrier	Expt	Calc
Ar	1	170	163	172		-2	20		42
	2	190	191	219	-29	-29			49
$(Ar)_2$[b]	1	444	443	480		-36	88		55
	2	457	456	513	-55	-56			56
N_2	1	270[d]	270	278[f]		-8	150		55
	2	265[e]	316	354[g]	-124	-89		65	80
CH_4	1	245	238	250		-5	64		66
	2	261	260	298	-107	-27			77
CF_4	1	371	366	380		-9	500		58
	2	560	711	807	-141	-247		59?	76
$(CF_4)_2$[c]	1	1637		1922		-285			
	2	1666		2107	-299	-441			

[a]Notation: E_B = ground state binding energy; E_B^* = electronic excited state binding energy; $p1$ = values obtained using only ground state potential parameters (α_i and r_i) but both ground and excited state charges and geometries; $p2$ = values obtained using both ground and excited state parameters (α_i and r_i), charges, and geometries. See Eqs. (1) and (2). Barrier = calculated potential energy barrier for the isomerization process, Shift = cluster spectral shift = $E_{mole} - E_{clust} = E_B - E_B^*$; and σ = excited state stretching mode energy calc = calculated value for the excited state).
[b]E_B for Ar dimer = 99 cm^{-1}. E_B = ground state binding energy.
[c]E_B for CF$_4$ dimer = 732 cm^{-1}.
[d]Value obtained without quadrupolar moment simulation, 213 cm^{-1}.
[e]Value obtained without quadrupolar moment simulation, 236 cm^{-1}.
[f]Value obtained without quadrupolar moment simulation, 205 cm^{-1}.
[g]Value obtained without quadrupolar moment simulation, 237 cm^{-1}.

TABLE III. Rotational constants (in cm^{-1}) for both ground and excited electronic states of the different clusters studied. The constants are obtained from the calculated geometries with the atom–atom potential program. These constants are used for the rotational contour simulation (see text and Figs. 4, 7, 10, 13).

CH_3O/X	Isomer	Ground state			Excited state		
		A	B	C	A	B	C
Ar	1	5.195	0.0492	0.0492	4.910	0.0121	0.0121
	2	0.940	0.0761	0.0714	0.750	0.0791	0.0726
$(Ar)_2$	1	0.0776	0.0479	0.0298	0.0808	0.0467	0.0298
	2	0.0760	0.0560	0.0342	0.0776	0.0551	0.0348
N_2	1	5.190	0.0500	0.0500	4.907	0.0477	0.0477
	2	0.789	0.0802	0.0739	0.615	0.963	0.0847
CH_4	1	2.594	0.0787	0.0787	2.455	0.0744	0.0744
	2	0.792	0.122	0.110	0.650	0.126	0.110
CF_4	1	0.183	0.0303	0.0303	0.183	0.0241	0.0241
	1	0.160	0.0470	0.0454	0.155	0.0488	0.0466
$(CF_4)_2$	1	0.0384	0.0205	0.0156	0.0400	0.0204	0.0157
	2	0.0388	0.0209	0.0162	0.0433	0.0182	0.0152

clusters. In Fig. 2 we see that only one of these isomers (probably the calculated most stable one) is present in the spectrum, at least for $CH_3(Ar)_1$. In order to determine which of the calculated isomers corresponds to the experimental spectrum, a rotational line shape simulation using the rotational constants from geometries given in Figs. 3(a) and 3(b) (see Table III) is performed. The theoretical rotational contours, together with the experimental line shape for $CH_3O(Ar)_1$ $\overline{3}{}_0^1$, are shown in Fig. 4. The $\overline{3}{}_0^1$ $CH_3O(Ar)_1$ vibration is chosen for the comparison instead of the $\overline{0}{}_0^0$ because it generates more intense signals and better cluster
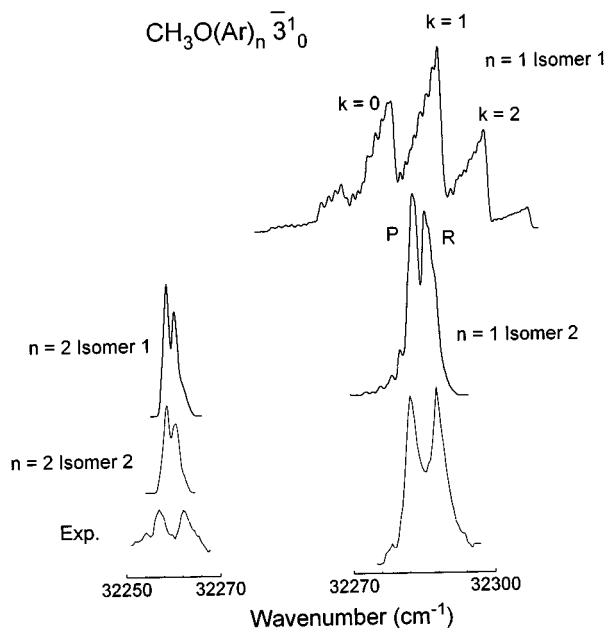
and van der Waals radii, so Eqs. (1) and (2) cannot be properly applied with appropriate parameters for excited state CH_3O. To address this difficulty, an estimation of the unknown CH_3O excited state polarizabilities and van der Waals radii is generated, using as a reference the ground state values and the experimental spectral shift for $CH_3O(Ar)_1$ isomer 2 (this assumes that the experimental spectrum corresponds to this cluster, a fact that will be confirmed below). We assume that upon excitation, the oxygen atom parameters will change more than the carbon atom parameters and that the hydrogen parameters are unchanged because the excitation represents promotion of an electron from the CO bond σ, π-system to a pure oxygen p orbital. Taking these assumptions, a change of $\sim +20\%$ for the oxygen and a change of $\sim +7\%$ for the carbon polarizabilities and van der Waals radii are required to achieve the desired cluster shift for $CH_3O(Ar)_1$. These new values of α and r (see Table I) are used without further modification in the rest of the calculations, including those for $CH_3O(Ar)_2$. All the rotational line shape simulations improve their agreement with the experimental result after using the new set of parameters to calculate cluster geometries.

The atom–atom potential calculations generate two different isomers with similar binding energies for all the 1:1

FIG. 4. Comparison between experimental and simulated rotational contours for $CH_3O(Ar)_n$, $n = 1, 2$, $\overline{3}{}_0^1$ transition. The comparison supports the assignment of the $CH_3O(Ar)_1$ spectrum to the calculated isomer 2. The comparison is not so useful for $CH_3O(Ar)_2$, due to the similarity between isomer 1 and isomer 2 calculated rotational contours.

spectra. The $CH_3O(Ar)_1$ 2_0^1 transitions cannot be compared to a calculated line shape because of its coincidence with the CH_3O 3_0^2 feature. This coincidence is not found for the rest of the clusters and this peak is the one that leads to higher signal/noise ratios; however, in order to follow a systematic procedure, all the comparisons between theoretical and experimental traces will be shown using $CH_3O(X)_n$ 3_0^1 transition.

Figure 4 shows good agreement between the rotational simulation for isomer 2 and the experiment line shape; the isomer 1 simulation is totally different from the experimental result. We can conclude that the observed cluster spectrum corresponds to $CH_3O(Ar)_1$ isomer 2. We do not know if only one isomer forms in the expansion or if both form, but the higher energy one surmounts the 20 cm^{-1} barrier (calculated, see Table II) separating the two theoretical isomers during the cooling process and the $CH_3O(Ar)_1$ clusters then remain in the lower energy structure.

For the $CH_3O(Ar)_2$ cluster, calculations again yield to two different isomers [see Figs. 3(c) and 3(d)] with calculated binding energies of 444 cm^{-1} for isomer 1 and 457 for isomer 2. In isomer 1, one of the Ar atoms is placed close to the oxygen, attracted to the C–O bond electron density, with the second one close to two of the CH_3O H atoms. Both Ar atoms are on the same side of the CH_3O. In isomer 2 [see Fig. 3(d)] both Ar atoms are attracted to the C–O bond. Each Ar atom position with respect to the C–O bond is very similar to the Ar atom position for the 1:1 cluster isomer 1 [see Fig. 3(b)]. Using the corrected parameters from the $CH_3O(Ar)_1$ calculation, we obtain excited state binding energies of 480 cm^{-1} and 513 cm^{-1} for isomers 1 and 2, respectively. This leads to predicted red shifts of -36 and -56 cm^{-1} for isomers 1 and 2, with isomer 2 in good agreement with the experimental value of -55 cm^{-1}. The data seem to confirm that the experimental spectrum belongs to isomer 2. A further test is given by the rotational simulation (Fig. 4). As can be seen, the simulated rotational contours for isomer 1 and isomer 2 are almost identical. The rotational simulation is successful in reproducing the double peak of the experimental spectrum, but is not able to reproduce the separation between peaks (5 cm^{-1} in the experimental spectrum, only 2 cm^{-1} in the simulated one). This can be due to small differences between the calculated positions of the Ar atoms and the actual ones. The potential of these highly dynamic, weakly bound complexes is so shallow that a difference of ± 0.1 Å in the relative position of the species comprising the cluster does not change the binding energy, but is sufficient to change the rotational constants. For example, in $CH_3O(Ar)_2$, a change of ~ 0.15 Å in the position of one of the Ar atoms, leads to a change of only ~ 0.8 cm^{-1} in the binding energy, but a 5%–8% change in the rotational constants. The same type of very shallow potentials have been found in other clusters, for example, OH–Ar,[7] OH–Ne, and OD–Ne.[40]

In summary, we find theoretically two different isomers for $CH_3(Ar)_1$ and $CH_3O(Ar)_2$ clusters, with very similar binding energies. In both cases, only one of these isomers appears in the experimental spectra, the calculated most
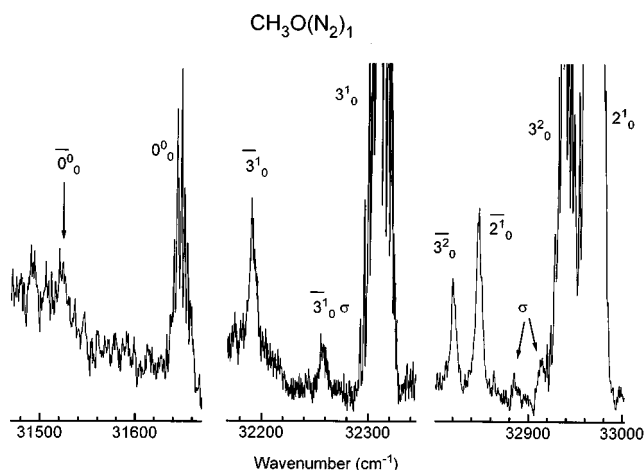

FIG. 5. LIF spectra of $CH_3O(N_2)_1$ in the vicinity of four different CH_3O vibratonic features, 0_0^0, 3_0^1, 3_0^2, and 2_0^1.

stable one. The rotational contour simulation for $CH_3O(Ar)_1$ strongly supports the atom–atom potential calculations; but for $CH_3O(Ar)_2$ the similarity between the simulated spectra of both isomers makes this calculation inconclusive. We assume that only the most stable calculated isomer generates the 1:2 cluster spectrum.

C. Methoxy/nitrogen

Figure 5 depicts the $CH_3O(N_2)_1$ spectrum for the $\overline{0}_0^0$, $\overline{3}_0^1$, $\overline{3}_0^2$, and $\overline{2}_0^1$ transitions. The spectrum consists of peaks red shifted by ~ -124 cm^{-1} with respect to the bare molecule features. The shifts are almost identical for all the CH_3O vibrations (between -125 and -122 cm^{-1}, see Table IV) as is found for $CH_3O(Ar)_n$ clusters (see Table IV). It is possible for three of the vibrations ($\overline{3}_0^1$, $\overline{3}_0^2$, and $\overline{2}_0^1$) to distinguish a weak cluster feature 65 cm^{-1} from the main one, with a similar shape. This peak is probably due to the cluster vibronic (σ) transition involving the stretching vibration in the excited state.

Calculation of $CH_3O(N_2)_1$ cluster structure requires the introduction of the well-known N_2 quadrupole moment by adding a pair of charges (see Table I) on the N_2 molecular

TABLE IV. Experimental shifts and excited state stretching mode energies (cm^{-1}) observed for each cluster as a function of vibronic features of CH_3O.

Cluster	$\overline{0}_0^0$		$\overline{3}_0^1$		$\overline{3}_0^2$		$\overline{2}_0^1$	
	shift	σ	shift	σ	shift	σ	shift	σ
Ar	28		29		28			
(Ar)$_2$	59		55					
N$_2$	124		125	65	122	65	124	65
CH$_4$			107				109	
CF$_4$	138		141	59[a]	141	58[b]	141	[c]
(CF$_4$)$_2$			299				299	

[a]Other vibration at 24 cm^{-1}.
[b]Other vibrations at 14 and 24 cm^{-1}.
[c]Other vibration at 15 cm^{-1}.

$CH_3O(N_2)_1$

Isomer 1, E_B= 270 cm^{-1} Isomer 2, E_B= 265 cm^{-1}
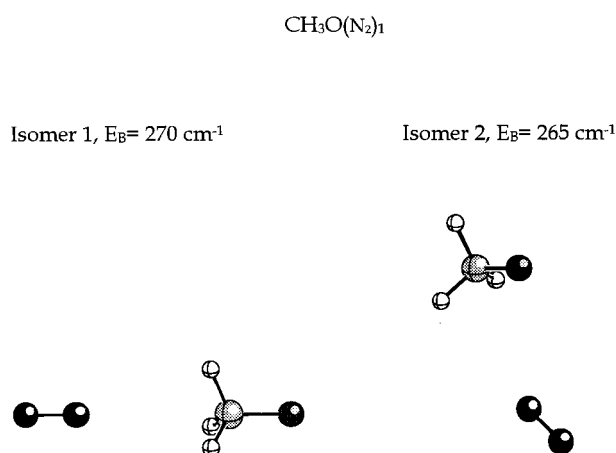
FIG. 6. Calculated structures for $CH_3O(N_2)_1$ isomers 1 and 2.

$CH_3O(N_2)_1$ $\overline{3}^1_0$

a. Isomer 1

b. Isomer 2

c. Exp.

32160   32180   32200   32220

Wavenumber (cm^{-1})

FIG. 7. Comparison between experimental and simulated rotational contours for the $CH_3O(N_2)_1$ $\overline{3}^1_0$ transition. The comparison supports the assignment of $CH_3O(N_2)_1$ spectrum to isomer 2.

axis as indicated in Table I. Again the atom–atom potential calculation leads to two different isomers (see Fig. 6). The structure labeled as isomer 1 (E_B=270 cm^{-1}) has the N_2 molecule attached to the H atom end of CH_3O, with its molecular axis coincident with the CH_3O molecular axis. This structure resembles the one found for $CH_3O(Ar)_1$ isomer 1 [see Fig. 3(a)].

In isomer 2, the N_2 molecule lies in the plane formed by the C and O atoms and one of the H atoms, with the N_2 molecular axis forming an angle of ~46° with the CH_3O molecular axis. A projection of the N_2 molecule bond axis on the C–O bond is centered on the O atom, suggesting that one of the N atoms is coordinated to both the C and O atoms of CH_3O. The other N atom is away from the CH_3 end of the CH_3O radical as depicted in Fig. 6. The binding energy for isomer 2 (E_B=265 cm^{-1}) is slightly smaller than for isomer 1 (only 5 cm^{-1}, see Table II). Excited state isomer 2 is, however, more tightly bound than is isomer 1 (E_B^* =354 cm^{-1} for isomer 2 compared with the E_B^*=278 cm^{-1} for isomer 1). The calculated shift for isomer 2 is closer to the experimental one than that for isomer 1 (see Table II).

The atom–atom potential energy calculation suggests that isomer 1 is the most stable structure, but the experimental shift (-124 cm^{-1}) is closer to the calculated one for isomer 2 (-89 cm^{-1}) than to the one for isomer 1 (-8 cm^{-1}). Assuming that the peak at 65 cm^{-1} corresponds to the stretching vibration, this value lies halfway between the calculated excited state stretching frequencies of isomer 1 (55 cm^{-1}) and isomer 2 (80 cm^{-1}).

The rotational simulation in Fig. 7 shows good agreement between the isomer 2 rotational contour and the $\overline{3}^1_0$ experimental one. The agreement between simulated and experimental spectra is even better for $CH_3O(N_2)_1$ $\overline{3}^2_0$ and $\overline{2}^1_0$ peaks, but as explained above, the comparison between simulated and experimental rotational contours will be always done for the $CH_3O(X)_n$ $\overline{3}^1_0$ peak.

While the atom–atom potential calculations indicate that isomer 1 is slightly more stable, rotational simulations indicate that the spectra shown in Fig. 5 correspond to
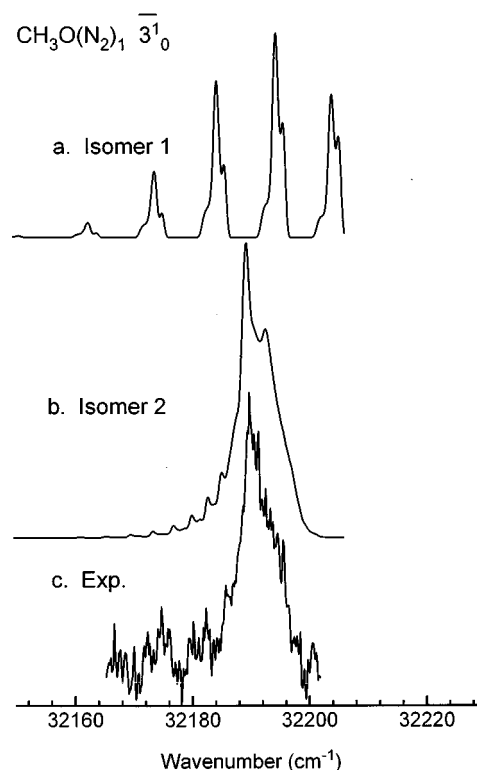
$CH_3O(N_2)_1$ isomer 2; either isomer 1 is not stable in the expansion or its spectrum is not detected. The ground electronic state binding energy could be overestimated by the additional charges employed to simulate the N_2 quadrupole moment. If the charges are not employed, isomer 2 is more stable by ~20 cm^{-1}; the calculated shifts are much worse without the N_2 quadrupole addition to the potential function, however.

D. Methoxy/methane

The low signal intensity obtained for the $CH_3O(CH_4)_1$ cluster prevents its detection at the weak 0^0_0 transition; in Fig. 8 only the spectra for 3^1_0 and 3^2_0 and 2^0_1 CH_3O transitions are shown. The spectra consist of only one relatively broad cluster peak (FWHH~10 cm^{-1}) for each CH_3O vibronic transition. No peaks due to possible cluster van der Waals vibrations can be positively identified. Atom–atom potential calculations predict two different structures for this cluster (see Fig. 9), and both are very similar to those obtained for the $CH_3O(Ar)_1$ and $CH_3O(N_2)_1$ systems. In isomer 1 the methane molecule is attached to the H end of the CH_3O radical. The CH_4 H atoms are in a staggered conformation with those of CH_3O and the CH_4 C atom is on the CH_3O molecular axis. In isomer 2, the CH_4 molecule is attracted by the charge density in the C–O bond. Two of its H atoms and the carbon atom lie in the plane formed by the radical C–O bond and one of the CH_3 H atoms. This plane becomes a symmetry plane for the cluster. Both clusters have similar
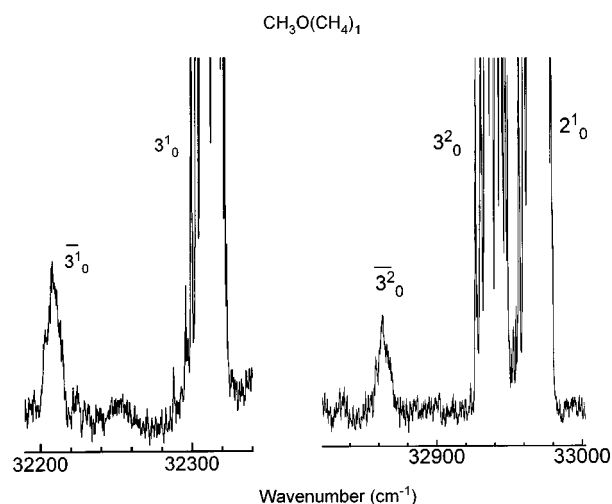
FIG. 8. LIF spectra of $CH_3O(CH_4)_1$ in the vicinity of three different CH_3O vibrations, 3^1_0, 3^2_0, and 2^1_0. The poor signal intensity prevents for recording the spectrum at the CH_3O origin.

binding energies, but isomer 2 is somewhat more stable than isomer 1 ($E_B = 261$ cm^{-1} compared with 245 cm^{-1} for isomer 1).

The calculated and experimental shifts, however, show a lack of agreement; the experimental shift is about four times larger than that calculated for isomer 2 (the most stable one). The use of corrected $\alpha_i s$ and $r_i s$ improves the excited state calculation (see Table II) only slightly. The intermolecular interaction for CH_3O/CH_4 in the excited CH_3O A^2A_1 state is apparently underestimated by at least 100 cm^{-1}. One possibility for this enhanced interaction is the existence of a reactive interaction between CH_4 and CH_3O, such that the reaction

$$CH_3O + CH_4 \rightarrow CH_3OH + CH_3 \tag{3}$$

begins to occur.

$CH_3O(CH_4)_1$
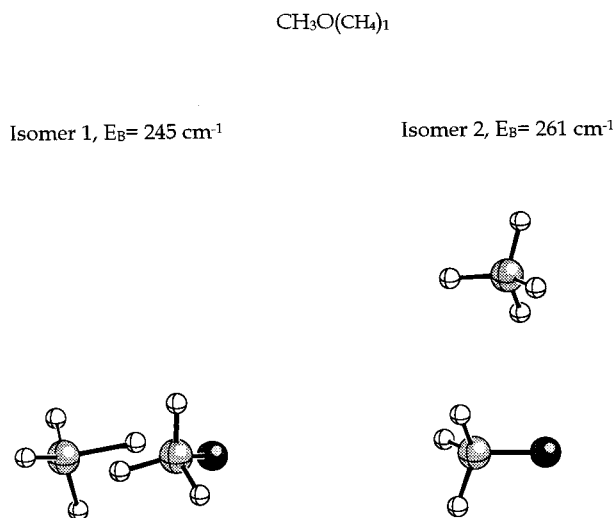

Isomer 1, E_B= 245 cm^{-1} Isomer 2, E_B= 261 cm^{-1}

FIG. 9. Calculated structures for $CH_3O(CH_4)_1$ isomers 1 and 2.
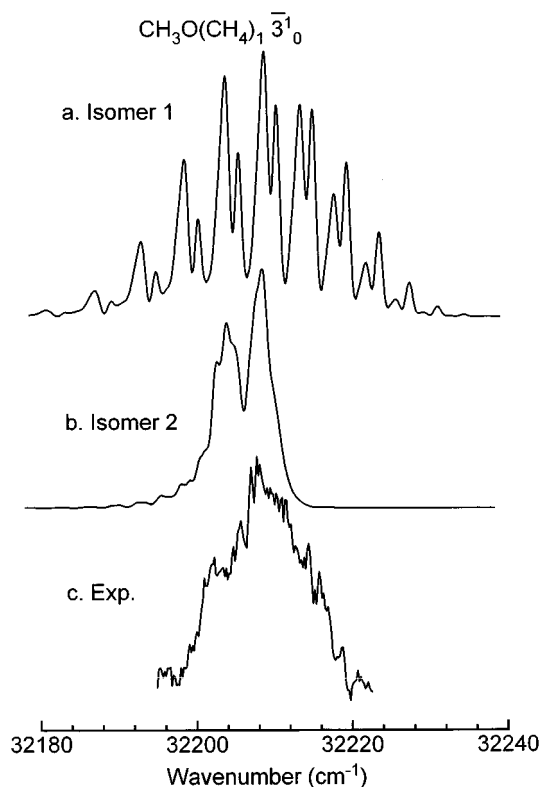

FIG. 10. Comparison between experimental and simulated rotational contours for the $CH_3O(CH_4)_1$ $\overline{3}^1_0$ transition. The comparison suggests the assignment of $CH_3O(CH_4)_1$ spectrum to isomer 2.

Wantuck et al.[41] found reaction (3) to be very slow for the CH_3O ground state, with an upper limit for the reaction rate constant $< 10^{-15}$ cm^3 molec^{-1} s^{-1} at room temperature. A different situation is presented for the excited state. In the same work, a disappearance rate constant for the CH_3O $^2A_1$ state with CH_4 of $1.05 \pm 0.07 \times 10^{-10}$ cm^{3}molec^{-1} s^{-1} is found. This rate is 10^3 times higher than the constant for collisional quenching with CF_4: $1.40 \pm 0.05 \times 10^{-13}$. The processes that can remove $CH_3O(^2A_1)$ are

$$CH_3O(^2A_1) + CH_4 \rightarrow CH_3O(X) + CH_4 \tag{4}$$

$$\rightarrow CH_3OH + CH_3. \tag{5}$$
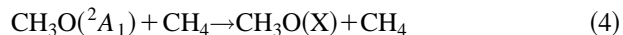
Making a comparison with the same reactions for OH,[42] Wantuck et al. concluded that the high disappearance constant is due to a reactive contribution [i.e., Eq. (5)].

If such a reaction is a reality, the cluster must be formed in the reactive entrance channel, far away from the transition state. Otherwise, the cluster spectrum should be broad, as found for benzyl radical/ethylene system.[22] A comparison between the simulated and experimental rotational contours (Fig. 10) shows that the experimental spectrum is broader and less well resolved than the calculated one for isomer 2; nonetheless, the calculated isomer 2 is clearly the proper structure based on the shift and rotational contour calculations.

No CH_3O clusters are detected with the solvent molecules CF_3H, C_2H_6, C_3H_8, and CO_2. The reactions cross sections for all these molecules are larger than that for CH_4.[42]

The same type of potential energy calculations have been carried out for the benzyl radical $(CH_4)_1$ cluster.[22] In this latter instance the agreement between calculated and experiment shifts are excellent; the calculated shift is -35 cm^{-1} and the observed shifts are between -29 cm^{-1} and -39 cm^{-1}, depending on the vibronic feature accessed. The most remarkable difference between the benzyl radical $(CH_4)_1$ and $CH_3O(CH_4)_1$ clusters is that in the first case a reaction is not anticipated while in the second case one is anticipated.

In order to perform a further test on this reaction hypothesis an effort has been undertaken to detect the products from reaction (5) (CH_3OH and CH_3). This detection has not been possible with the LIF technique, because the CH_3OH and CH_3 absorption bands lie in the vacuum ultraviolet, beyond the range of our photomultiplier tubes, so an attempt to identify CH_3O and its clusters through mass detection was initiated. To the best of our knowledge, the only observation of CH_3O by mass detection is due to Long et al.[43] using a Rydberg state and a $2+1$ REMPI process. To date, no REMPI spectrum using the A state in conjunction with mass detection has been published. We can repeat the results of Ref. 43, but we could not detect CH_3O from $1+2$ REMPI process employing the A state. Additionally, a number of fragments are detected; the same Rydberg state spectrum can be recorded using mass channels 31 (CH_3O) and 29 (HCO). We suggest that the reason the $1+2$ REMPI ionization and subsequent mass detection of CH_3, CH_3O, HCO, etc., does not yield a spectrum of the $A\ {}^2A_1$ state is very rapid relaxation processes at the resonant intermediate state generated by the second photon absorption. We have tried to tune the laser to different spectral regions, but to no avail. Perhaps a ~ 100 fs laser pulse could generate such mass detected radical and cluster spectra.

E. Methoxy/tetrafluoromethane

$CH_3O(CF_4)_1$ is the strongest bound cluster of the four studied in this work. The interactions between the electronegative fluorine atoms and the electron density surrounding the C–O bond leads to high binding energies and large cluster shifts. Figure 11 shows the $CH_3O(CF_4)_1$ spectra at the 0_0^0, 3_0^1, 3_0^2, and 2_0^1 CH_3O transitions. In two of the regions (vibrations 3_0^1 and 3_0^2 and 2_0^1), the spectrum is composed of a few features, but for the origin, due to the weaker signal, only one cluster transition is observed. According to the pressure behavior of the different peaks, we assign the double peaks at 32 016 and 32 673 cm^{-1} as due to the $CH_3O(CF_4)_2$ cluster and the rest of the non-CH_3O transitions as belonging to the 1:1 cluster. The shift is almost the same for all the bare molecule vibrations; ~ 141 cm^{-1} for the 1:1 cluster and 298 cm^{-1} for the 1:2.

As with the other CH_3O/solvent clusters, the atom–atom potential calculations for $CH_3O(CF_4)_1$ lead to two different
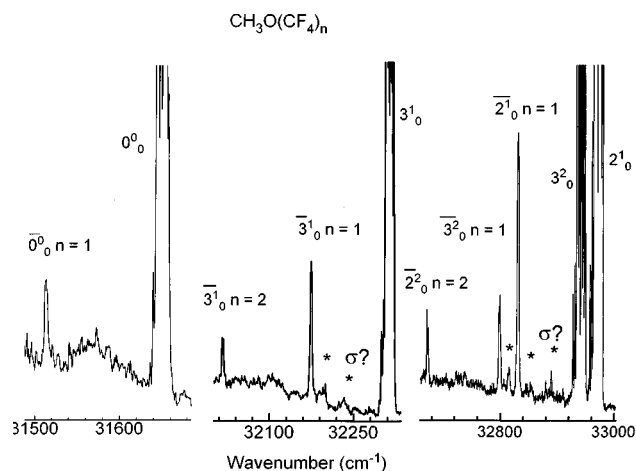

FIG. 11. LIF spectra of $CH_3O(CF_4)1$ in the vicinity of four different CH_3O vibronic features, 0_0^0, 3_0^1, 3_0^2, and 2_0^1.

structures, depicted in Fig. 12. Isomer 1 has a very similar structure to that for $CH_3O(CH_4)_1$ isomer 1; the CF_4 molecule is attracted by the CH_3O H atoms. The CF_4 C atom and one of the fluorine atoms are over the CH_3O molecular axis with this C–F bond pointing to the CH_3O C atom. The rest of the fluorine atoms are in an eclipsed conformation with respect to the CH_3O H atoms. The main differences between $CH_3O(CF_4)_1$ and $CH_3O(CH_4)_1$ isomer 1 structures are that the C atom of the CH_4 is on the CH_3O molecular axis and that three CH_4 H atoms are staggered with respect to the CH_3O H atoms.

The $CH_3O(CF_4)_1$ isomer 2 structure is also very similar to that of the $CH_3O(CH_4)_1$ isomer 2, but in this case the solvent molecule is tilted, such that one of the C–F bonds points toward the CH_3O C atom, rather than a C–F bond being parallel to the C–O bond. According to the calculation, this is the more stable isomer ($E_B = 560$ cm^{-1} compared with $E_B = 371$ cm^{-1} for isomer 1, see Table II).

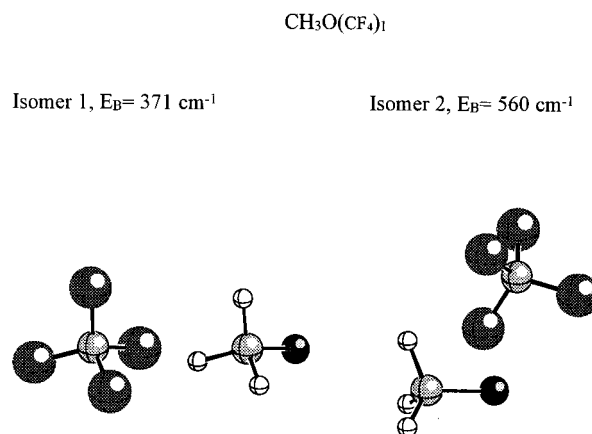A comparison between experimental and calculated shifts shows a poor agreement, however. The experimental

FIG. 12. Calculated structures for the $CH_3O(CF_4)_1$ isomers 1 and 2.

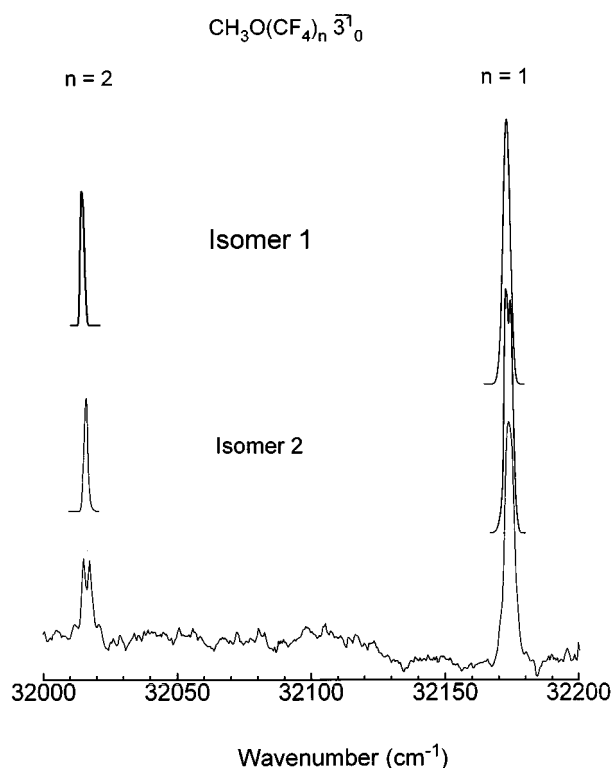$CH_3O(CF_4)_n \; \overline{3}{}^1_0$

n = 2   n = 1

Isomer 1

Isomer 2

32000   32050   32100   32150   32200

Wavenumber (cm^{-1})

FIG. 13. Comparison between experimental and simulated rotational contours for the $CH_3O(CF_4)_n$ ($n=1,2$) $\overline{3}{}^1_0$ transitions. The simulation is not helpful for assignment of cluster structure, due to the similarity of the rotational contours for both isomers.

$CH_3O(CF_4)_2$

Isomer 1, E_B= 1637 cm^{-1} Isomer 2, E_B= 1666 cm^{-1}

Isomer 3, E_B= 1427 cm^{-1} Isomer 4, E_B= 1135 cm^{-1}

Isomer 5, E_B= 1097 cm^{-1}

FIG. 14. Calculated structure for five different isomers of $CH_3O(CF_4)_2$. The strong interaction between CF_4 molecules suggests a structural model of the CF_4 dimer solvating the CH_3O radical. This limiting structure is particularly obvious for isomers 4 and 5 but can be envisioned for all the isomers.

value, -140 cm^{-1}, is $\sim 100 \text{ cm}^{-1}$ smaller than the calculated shift for isomer 2 (-247 cm^{-1}) and about 130 cm^{-1} larger than the calculated shift for isomer 1 (-9 cm^{-1}); the excited state intermolecular interaction seems to be overestimated for this cluster if indeed isomer 2 is the accepted cluster structure.

A comparison between calculated and experimental values for the stretching vibration shows a good agreement between the calculated isomer 1 stretching mode and the experimental value (58 compared to 59 cm^{-1}), while the value for the stretching mode of isomer 2 is too large (76 cm^{-1}). But as the binding energy for the excited state of isomer 2 seems to be overestimated, one can expect that the calculated vibrational frequencies of isomer 2 would be too large, as well.

The rotational envelope simulation for the vibronic bands of this cluster is not useful for determining cluster structure. If one visualizes the cluster as a big mass (the CF_4 molecule) with a small mass (the CH_3O radical) attached to it in two possible ways, one sees that the two different isomers should have very similar rotational constants (see Table III). As can be seen in Fig. 13, the rotational envelope simulation for both isomers is almost identical. We assume that the spectrum corresponds to $CH_3O(CF_4)_1$ isomer 2 because of the calculated large ground state binding energy for this cluster.
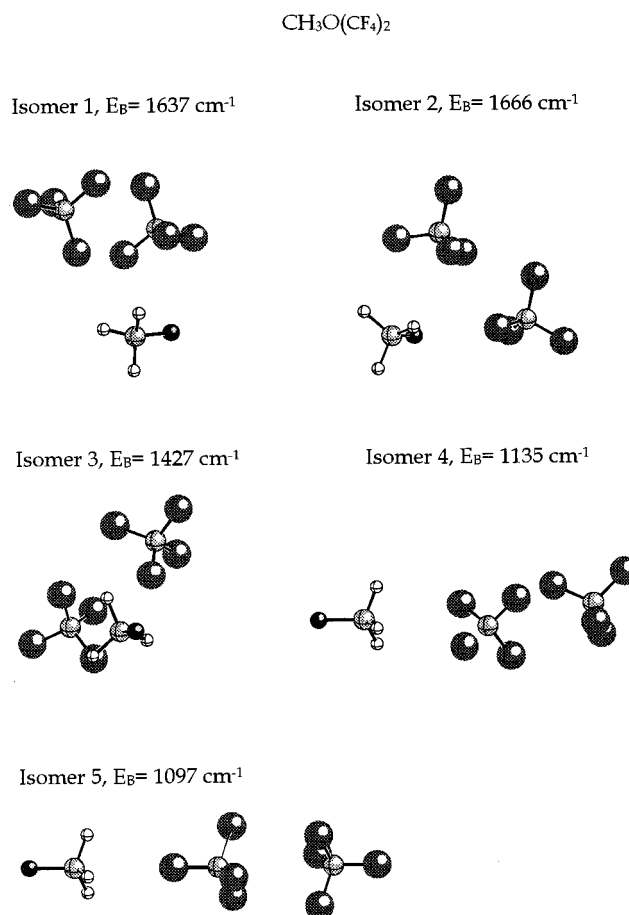
The calculations show a large number of stable geom-

etries for $CH_3O(CF_4)_2$. The difference between this cluster and $CH_3O(Ar)_2$ is that now the CF_4–CF_4 interaction (calculated $E_B = 732 \text{ cm}^{-1}$) is comparable to (actually is larger than) the CH_3O–CF_4 one. The five main isomers for the $CH_3O(CF_4)_2$ cluster are shown in Fig. 14. Isomer 1 and 2 (the most stable ones, with binding energies of 1637 and 1666 cm^{-1}) resemble the structure found for $CH_3O(Ar)_2$ [see Figs. 3(c) and 3(d)]. Two of the isomers (3 and 4) clearly show that CF_4 molecules coordinate and only one of them interacts with the CH_3O radical. The isomer 5 binding energy (1097 cm^{-1}) is very nearly the sum of CH_3O–CF_4 isomer 1 (371 cm^{-1}) and CF_4–CF_4 interactions (732 cm^{-1}).

Again, the rotational simulation is of little help here (see Fig. 13) and it is not successful in reproducing the double peak found in the experimental spectrum. Thus we assume that the experimental spectrum corresponds, as for the rest of the clusters, with the calculated most stable $CH_3O(CF_4)_2$ isomer 2 cluster.

IV. DISCUSSION

All the solvent molecules used in this study are nonpolar. The clusters between them and the CH_3O radicals

present significant structural similarities. For all the 1:1 clusters, two different isomers are found; isomer 1 has the solvent molecule attracted to the H atom end of the CH_3O radical; and isomer 2 has the solvent molecule attracted by the charge density around the C–O bond. In all the clusters but one $[CH_3O(N_2)_1]$, isomer 2 is the energetically most stable conformer for the ground electronic state. For $CH_3O(N_2)_1$, a pair of charges are introduced at 0.25 Å from each N_2 atom (on the bond axis) in order to simulate the N_2 quadrupole moment (see Tables I and II). In this instance we choose cluster isomer 2 as the observed one based on the cluster shift calculation, the rotational contour simulation, and the overall systematics of this series of CH_3O/solvent clusters.

The $CH_3O(X)_2$ clusters also seem to evidence a systematic class of structures. A comparison of $CH_3O(Ar)_2$ and $CH_3O(CF_4)_2$ isomers 1 and 2 shows that, in both sets of clusters, the solvent molecules are placed in similar positions.

Despite the nearly degenerate ground state binding energies for some of the cluster isomers [e.g., $CH_3O(Ar)_1$ and $CH_3O(N_2)_1$], only one of the isomers is detected for each solvent. This observation can be explained in two different ways. For the isomers with low potential energy barriers for the isomerization process, the less stable isomer can have enough energy during the cooling process to undergo isomerization. This is, for example, the situation for $CH_3O(Ar)_1$ and $CH_3O(CH_4)_1$. For the rest of the clusters, the stabilization energy difference between the two isomers is large enough such that formation of only the more stable isomer can occur directly in the expansion.

The cluster shifts for all isomer 1 clusters are quite small (see Table II). This relates to their structural similarity and the fact that the redistribution of electron density associated with electronic excitation occurs mostly for the C–O bond region of the CH_3O radical. Isomer 1 clusters all have the solvent molecule coordinated to the hydrogen atom end of the CH_3O for which the electron density changes very little upon electronic $A \leftarrow X$ excitation.

As can be seen in Table IV, the spectral shifts found for all the clusters do not depend on the bare molecule vibrational excitation. This means that the increasing of the bare molecule vibrational excitation does not affect the cluster binding energy. This behavior has been found in other small radical/solvent clusters [for example, $OH(Ar_1)$ (Ref. 44) and vinoxy $(Ar)_1$ (Ref. 45)]. This behavior indicates that the structural changes produced in the bare molecule due to the vibrational excitation do not affect the binding energy of the cluster. The similarity (within the present spectral resolution) between the rotational contours for peaks of different transitions indicates that the averaged cluster geometry itself is not affected by the bare molecule vibrational excitation. The cluster binding energy also does not seem to be greatly affected by the large change in C–O bond length ($\sim +0.2$ Å) produced upon electronic excitation. This can be verified from Table II by comparing columns E_B and E_B^*. The change in the binding energy from ground to the electronic excited state is due mainly to a change in the atomic partial charge, polarizabilities and van der Waals radii of the C and

O atoms. The absence for most of the clusters of van der Waals progressions additionally indicates vertical transitions with Franck–Condon Factors favoring the $\overline{0}\,^0_0$ transition.

The above similarities notwithstanding, the form of the interaction (specifically the potential energy function) that governs the details of cluster geometry in each cluster is somewhat different. The main interaction for the CH_3O/Ar system is dispersion because the Ar atom has no charge. Excited state behavior for this cluster is characterized by changing the C and O polarizabilities and van der Waals radii. If these values are not changed, essentially no change in binding energy is found upon electronic excitation; that is, the cluster shift is zero.

The opposite behavior is found for CH_3O/CF_4 clusters. As can be seen in Table II, the electronic excited state binding energy calculation using the uncorrected parameters α_i and r_i (taking into account only the change in the binding energy due to the electrostatic term and to the change in the CH_3O geometry) is 711 cm^{-1} for isomer 2; i.e., 151 cm^{-1} larger than for the ground state. The introduction of the correction to the parameters increases the excited state binding only 86 cm^{-1}; thus the CH_3O/CF_4 cluster is more tightly bound in the excited state due mainly to an increase in the electrostatic interaction between the molecules.

The N_2 quadrupole moment interactions govern the cluster geometry for the CH_3O/N_2 system. If the quadrupole moment is not considered (that is, if the extra charges are not added to the N_2 molecule in the cluster), a cluster shift of only -1 cm^{-1} is found for isomer 2 (compared with the experimental value of -124 cm^{-1}). The introduction of the quadrupole moment not only increases the binding energy and shift, but also modifies the cluster geometry by shortening the distance between solute and solvent species. This geometry change further increases the effect of changes in α_i and r_i for the excited state binding energy; the new parameters contribute 38 cm^{-1} to the total calculated shift (compared with 1 cm^{-1} before the introduction of the quadrupole moment).

Finally, the calculated spectral shift found for CH_3O/CH_4 is ~ 4 times smaller than the experimental value. As pointed out in Sec. III, the main reason for this large observed shift is the possible onset of a chemical reaction or bonding rearrangement.

The potential energy surface expression in Eq. (1) used here gives a good starting point for cluster geometry study and spectra analysis, but fails to give a quantitatively accurate result for (relative) binding energies.

The next step in complexity in these theoretical approaches is to use *ab initio* calculations; however, the weak character of the van der Waals bond makes this kind of calculations difficult to perform.[46] Problems such as basis set superposition error, basis set size, and enough CI are a constant concern. On the other hand, only clusters between small molecules are amenable to calculation with this algorithm due to the increase in time for and complexity of calculation with the increase in the number of atoms. Perhaps the best current *ab initio* approach involves large basis sets (double zeta plus polarization), CASSCF to account for degeneracy

problems, followed by either multireference CI or MP2 techniques.[47]

V. CONCLUSIONS

The structure of CH_3O clusters with Ar, $(Ar)_2$, N_2, CH_4, CF_4, and $(CF_4)_2$ has been elucidate. All the clusters present similar structures, with the solvent molecules placed closed to the C–O bond. The relative importance of the different interactions that contribute to the van der Waals bond [see Eq. (1)] are different for each cluster. In $CH_3O(Ar)_n$, the interaction is mainly dispersive. For $CH_3O(N_2)_1$, the dipolar–quadrupolar interaction plays an important role in the cluster bond. The main interaction between CF_4 and CH_3O is due to Coulombic attraction. Finally, the binding between CH_3O and CH_4 probably presents some reactive character.

Atom–atom potential calculations are shown to be quite useful for the determination of cluster structures, but are difficult to perform for open-shell systems especially for excited electronic states of the radical, as parameters are not available for the potentials. This problem can be partially solved using *ab initio* calculations. The combination of atom–atom potential calculation and rotational contour simulations allows one to determine cluster structure and to distinguish between the spectra of different cluster isomers. The calculation of cluster ground and excited state binding energies, as determined in this study through cluster spectroscopic shifts, is qualitatively, but not always quantitatively, correct.

ACKNOWLEDGMENTS

[1] (a) M. F. Hineman, S. K. Kim, E. R. Bernstein, and D. F. Kelley, J. Chem. Phys. **96**, 4904 (1992); (b) B. Coutant and P. Brechignac, *ibid.* **91**, 1978 (1989); (c) M. R. Nimlos, M. A. Young, E. R. Bernstein, and D. F. Kelley, *ibid.* **91**, 5268 (1989).

[2] (a) Y. Oshima, H. Koguchi, and Y. Endo, Chem. Phys. Lett. **184**, 21 (1991); (b) D. J. Nesbitt, Chem. Rev. **88**, 843 (1988); Faraday Discuss. **97**, 1 (1994); (c) T. G. Fraser, Int. Rev. Phys. Chem. **10**, 189 (1991).

[3] See, for example, (a) M. I. Lester, Adv. Chem. Phys. **46**, 51 (1996), and references therein; (b) R. Nowak, J. A. Menapace, and E. R. Bernstein, J. Chem. Phys. **89**, 1309 (1988); (c) S. Sun, and E. R. Bernstein, *ibid.* **103**, 4447 (1995); (d) Th. Weber, A. M. Smith, E. Riedle, J. H. Neuser, and E. W. Schlag, Chem. Phys. Lett. **175**, 79 (1990); (e) P. Hobza, Q. Bludsky, H. L. Selzle, and E. W. Schlag, J. Chem. Phys. **98**, 6223 (1993).

[4] See, for example, (a) E. R. Bernstein, K. Law, and M. Schauer, J. Chem. Phys. **80**, 207, 634 (1984); (b) J. L. Knee and P. M. Johnson, *ibid.* **80**, 13 (1984); (c) A. W. Garret and T. S. Zwier, *ibid.* **96**, 3402 (1992).

[5] D. Fulle, H. F. Hamann, H. Hippler, and J. Troe, J. Chem. Phys. **105**, 983 (1996).

[6] C. Chakravarty, D. C. Clary, A. D. Esposti, and H.-J. Werner, J. Chem. Phys. **95**, 8149 (1991); **93**, 3367 (1990).

[7] L. C. Giancarlo, R. W. Randall, S. E. Choi, and M. I. Lester, J. Chem. Phys. **101**, 2914 (1994).

[8] A. González-Lafonte and D. G. Trular, in *Chemical Reactions in Clusters*, edited by E. R. Bernstein (Oxford University Press, Oxford, 1996).

[9] S. Sun and E. R. Bernstein, J. Phys. Chem. **100**, 13 348 (1996).

[10] (a) C. M. Western, M. P. Casassas, and K. C. Janda, J. Chem. Phys. **80**, 4781 (1984); (b) W.-L. Lin, K. Kolenbrander, and J. M. Lisy, Chem. Phys.

[11] Lett. **112**, 585 (1984); A. C. Peet, D. C. Clary, and J. M. Hutson, J. Chem. Soc. Faraday Trans. 2 **83**, 1719 (1987).

[11] R. F. McGuire, F. A. Momany, and H. A. Scheraga, J. Phys. Chem. **76**, 375 (1972).

[12] G. C. Maitland, M. Rigby, E. B. Smith, and W. A. Wakeham, *Intermolecular Forces* (Oxford University Press, Oxford, 1981).

[13] N. Karasawa, S. Dasgupta, and W. A. Goddard, J. Phys. Chem. **95**, 2260 (1991).

[14] (a) A. D. Buckingham and P. W. Fowler, J. Chem. Phys. **79**, 6426 (1983); (b) G. J. B. Hurst, P. W. Fowler, A. J. Stone, and A. D. Buckingham, Int. J. Quantum Chem. **29**, 1223 (1986).

[15] (a) J. Goodman and L. E. Brus, J. Chem. Phys. **65**, 3146 (1976); **67**, 4858 (1977); (b) S. E. Novic, K. C. Janda, and W. Klemperer, *ibid.* **65**, 5115 (1976); (c) S. E. Novic, K. C. Janda, S. L. Holmgren, M. Waldman, and W. Klemperer, *ibid.* **65**, 1114 (1976).

[16] (a) R. Ahamad-Bitar, W. P. Lapatovich, D. E. Pritchard, and I. Renhom, Phys. Rev. Lett. **39**, 1657 (1997); (b) R. E. Smalley, D. A. Auerbach, P. S. H. Fitch, D. H. Levy, and L. Wharton, J. Chem. Phys. **66**, 3778 (1977); (c) R. R. Freeman, E. M. Mattison, D. E. Pritchard, and D. Kleppner, *ibid.* **64**, 1194 (1976); (d) M.-C. Duval, O. B. D'Azy, W. H. Breckenridge, C. Jouvet, and B. Soep, *ibid.* **85**, 6324 (1986); (e) J. Tellinguishen, Adv. Chem. Phys. **60**, 299 (1985).

[17] C. S. Dulcey and J. W. Hudgens, J. Chem. Phys. **84**, 5262 (1986), and references therein.

[18] (a) C. F. Jackels, J. Chem. Phys. **82**, 311 (1985); (b) **76**, 505 (1982).

[19] (a) D. L. Osborn, D. J. Leahy, E. M. Ross, and D. M. Neumark, Chem. Phys. Lett. **235**, 484 (1995); (b) A. Geers, J. Kappert, F. Temps, and J. W. Wiebrecht, J. Chem. Phys. **99**, 2271 (1993).

[20] (a) L. J. van der Burgt and M. C. Heaven, J. Chem. Phys. **89**, 2768 (1988); (b) M. T. Berry, M. R. Brustein, and M. I. Lester, *ibid.* **153**, 17 (1988); (c) G. W. Lemire, M. J. McQuaid, A. J. Kothlar, and R. C. Sausa, *ibid.* **99**, 91 (1993).

[21] R. Disselkamp and E. R. Bernstein, J. Chem. Phys. **98**, 4339 (1993).

[22] R. Disselkamp and E. R. Bernstein, J. Phys. Chem. **98**, 5260 (1994).

[23] *Introduction to Molecular Energy Transfer*, edited by J. T. Yardley (Academic, New York, 1980).

[24] (a) E. R. Bernstein, J. Chem. Phys. **52**, 5701 (1970); (b) M. Schauer and E. R. Bernstein, *ibid.* **82**, 3722 (1985).

[25] R. A. Scott and H. A. Scheraga, J. Chem. Phys. **45**, 2091 (1966).

[26] F. A. Momany, L. M. Carruthers, R. F. McGuire, and H. A. Scheraga, J. Chem. Phys. **778**, 1595 (1974).

[27] F. A. Momany, R. F. McGuire, A. W. Burgess, and H. A. Scheraga, J. Chem. Phys. **79**, 2361 (1975).

[28] G. Némethy, M. S. Pottle, and H. A. Scheraga, J. Chem. Phys. **87**, 1883 (1988).

[29] GAUSSIAN 94, M. J. Frisch, G. W. Trucks, H. B. Schlegel, P. M. W. Gill, B. G. Johnson, M. A. Robb, J. R. Cheeseman, T. A. Keith, G. A. Petersson, J. A. Montgomery, K. Raghavachari, M. A. Al-Laham, V. G. Zakrzewski, J. V. Ortiz, J. B. Foresman, J. Cioslowski, B. B. Stefanov, A. Nanayakkara, M. Challacombe, C. Y. Peng, P. Y. Ayala, W. Chen, M. W. Wong, J. L. Andrés, E. S. Replogle, R. Gomperts, R. L. Martin, D. J. Fox, J. S. Binkley, D. J. Defrees, J. Baker, J. P. Stewart, M. Head-Gordon, C. González, and J. A. Pople, Gaussian, Inc., Pittsburgh, Pennsylvania, 1995.

[30] E. B. Wilson, Jr., J. C. Decius, and P. C. Cross, *Molecular Vibrations, Theory of Infrared and Raman Vibrational Spectra* (McGraw–Hill, New York, 1955).

[31] J. A. Menapace and E. R. Bernstein, J. Phys. Chem. **91**, 2533 (1987).

[32] S. Li and E. R. Bernstein, J. Chem. Phys. **95**, 1577 (1991).

[33] (a) M. T. Martinez (private communication); (b) R. Pereira, A. Alava, F. Castaño, and M. T. Martínez, J. Chem. Soc. Faraday Trans. **90**, 2443 (1994); (c) R. Pereira, T. Calvo, F. Castaño, and M. T. Martínez, Chem. Phys. **201**, 433 (1995).

[34] X. Liu, C. P. Damo, T.-Y. D. Lin, S. C. Foster, P. Misra, L. Yu, and T. A. Miller, J. Phys. Chem. **93**, 2266 (1989).

[35] H. R. Wendt and H. E. Hunziker, J. Chem. Phys. **71**, 5202 (1979).

[36] D. L. Osborn, D. L. Leahy, E. M. Ross, and D. M. Neumark, Chem. Phys. Lett. **235**, 484 (1995).

[37] D. E. Powers, J. B. Hopkins, and R. E. Smalley, J. Chem. Phys. **85**, 2711 (1981).

[38] K. Fuke, K. Ozawa, and K. Kaya, Chem. Phys. Lett. **126**, 199 (1986).

[39] G. Herzberg, *Molecular Spectra and Molecular Structure*, Vol. III in *Electronic Spectra and Electronic Structure of Polyatomic Molecules* (Krieger, Malabar, 1991).

[40] Y. Lin, S. Fei, X. Zheng, and M. C. Heaven, J. Chem. Phys. **96**, 5020 (1992).

[41] P. J. Wantuck, R. C. Oldenborg, S. L. Baughcom, and K. R. Winn, J. Phys. Chem. **91**, 3253 (1987).

[42] (a) R. A. Copeland, M. J. Dyer, and D. R. Crosley, J. Chem. Phys. **82**, 4822 (1985); (b) R. A. Copeland and D. R. Crosley, *ibid*. **84**, 3099 (1986).

[43] G. R. Long, R. D. Johnson, and J. W. Hudgens, J. Phys. Chem. **90**, 4901 (1986).

[44] M. T. Berry, M. R. Brustein, and M. I. Lester, J. Chem. Phys. **92**, 6469 (1990).

[45] L. J. van de Burgt and M. C. Heaven, J. Chem. Phys. **89**, 2768 (1988).

[46] P. Hobza, H. L. Selzle, and E. W. Schlag, Chem. Rev. **94**, 1767 (1994).

[47] (a) P. Hobza, H. L. Selzle, and E. W. Schlag, J. Phys. Chem. **100**, 18 790 (1996); (b) C. Chipot, R. Jaffe, B. Maigret, D. A. Pearlman, and P. A. Kollman, J. Am. Chem. Soc. **118**, 11 217 (1996); (c) J. Sponer and P. Hobza, Chem. Phys. Lett. **267**, 263 (1997).